Collisional Evolution of the Main Asteroid Belt

William F. Bottke
Southwest Research Institute and the Institute for the Science of Exploration Targets (ISET), Boulder, CO

Miroslav Brož
Institute of Astronomy, Charles University, Prague

David P. O'Brien
Planetary Science Institute, ~~1700 E. Ft. Lowell, Suite 106,~~ Tucson, AZ

Adriano Campo Bagatin
Departamento de Fisica, Universidad de Alicante, Spain

Alessandro Morbidelli
Dep. Lagrange, CNRS, Observatoire de la Cote d'Azur, Universite de Nice Sophia-Antipolis; Nice, France

Simone Marchi
Southwest Research Institute and the Institute for the Science of Exploration Targets (ISET), Boulder, CO

Collisional and dynamical models of the main asteroid belt allow us to glean insights into planetesimal and planet formation scenarios as well as how the main belt reached its current state. Here we discuss the processes affecting small bodies and the constraints that can be used to test collisional model results. They indicate the main belt's wavy size-frequency distribution is a byproduct of comminution, with the shape a "fossil" of a violent early epoch. Most $D > 100$ km diameter asteroids are primordial, with their physical properties set by planetesimal formation and accretion processes. The main belt size distribution has evolved into a collisional steady state, and it has possibly been in that way for billions of years. Fragments constantly leave the main belt to produce a steady state near-Earth asteroid population by a combination of Yarkovsky/YORP ~~forces~~ and resonances. Asteroid families provide a critical record of main belt collisions, but heavily depleted and largely dispersed "ghost families" may hold the key to understanding the evolution of the primordial main belt.

effects

gravitational

1. INTRODUCTION

The main asteroid belt is a living relic. It contains a record of what happened to much of the Solar System since the planet formation epoch. Ongoing collisional and dynamical evolution processes, however, are slowly obscuring the traces left behind. The goal of modeling efforts is to use all possible observational data to discern the initial conditions and evolution processes that occurred during and after the planet formation epoch. For example, the questions one can probe with main belt constraints include the nature and mass of planetesimals inside of Jupiter's orbit, the timing of Jupiter's formation, the distribution of volatiles in the inner solar system, the size distribution produced during planetary accretion, the scaling laws that control collisional evolution both during and after planetary accretion, the presence of planetary embryos inside Jupiter's orbit, the migration of the giant planets and whether sweeping resonance ever crossed the main belt, the degree of material mixing that occurred between the feeding zones, etc.

A major uncertainty in any collisional evolution model of the asteroid belt concerns what happened when planet formation processes and/or giant planet migration was taking place. Many scenarios have been investigated over the last several decades, with the latest thinking discussed in the chapter by Morbidelli et al. . A key issue for many of them is the so-called mass deficit of the main belt (e.g., Morbidelli et al. 2009).

Consider that the total mass of the main asteroid belt, which is dominated by the masses of the largest asteroids, is $\sim 5 \times 10^{-4}$ Earth masses (Krasinsky et al. 2002; Somenzi et al. 2010; Kuchynka and Folkner 2013;). This value is tiny compared to the mass of solids thought to exist in the same region at the time of planetesimal formation. For example, the minimum mass solar nebula (Weidenschilling, 1977) suggests that 1-2.5 Earth masses of solid material once existed between 2 and 3 AU. If most of the solids ended up in planetesimals, the main belt region could potentially be deficient in mass by a factor $> 1,000$. Taken at face value, these values have been used to argue that the asteroid belt has lost more than 99.9% of its primordial mass

2. Processes Affecting Main Belt Evolution

Most collision evolution models involve the solution of a straightforward differential equation, though the details can be quite complicated and somewhat messy from an accounting standpoint. The input is an initial SFD for the asteroid belt ~~defined as (N)~~, with the bodies binned in logarithmic intervals as a function of diameter. The goal of the solution is to compute the time rate of change in the population per unit volume of space over a size range between diameter D and $D + dD$. In a schematic form, it can be written as:

$$\frac{\partial N}{\partial t}(D,t) = -I_{\rm COLL} + I_{\rm FRAG} - I_{\rm DYN}. \qquad (1)$$

Here $I_{\rm COLL}$ is the net number of bodies that leave between D and $D + dD$ per unit time from cratering or catastrophic disruption events. The net number of collisions taking place at every timestep is calculated by determining how many projectiles from other size bins are capable of producing either a cratering event (of interest) or a catastrophic disruption event among bodies between D and $D + dD$. Thus, this function is a "sink" for bodies in the SFD.

The results of the $I_{\rm COLL}$ calculation are sent to the function $I_{\rm FRAG}$, which describes the number of bodies entering a given size bin per unit time that were produced by the fragmentation of larger bodies. This allow large asteroids act as a reservoir for smaller bodies, with collisional evolution liberating them over time.

Finally, the equation accounts for $I_{\rm DYN}$, which is the number of bodies lost from a given size bin via dynamical processes, such as an object escaping through a dynamical resonance. This function is a sink for bodies in the SFD. Note that $I_{\rm DYN}$ is often enacted over the entire main belt SFD, which is reasonable for global dynamical mechanisms like sweeping resonances or migrating planets but is less accurate for bodies escaping from specific main belt regions via dynamical resonances (e.g., the ν_6 secular resonance along the inner edge of the maim belt; the 3:1 mean motion resonance with Jupiter at 2.5 AU).

In the sections below, we discuss the many parameters and mechanisms needed to understand and create these functions within a collision evolution model. We also discuss the possibility of including additional functions, such as allowing non-gravitational forces like YORP spin-up-driven mass shedding to act as an additional sink for small bodies (see chapter by Vokrouhlický et al.).

2.1 Asteroid Collision Probabilities

A necessary component to determining the collisional evolution of a population is to compute the impact probabilities and relative velocities between all possible pairs of bodies. These values are used to estimate the interval between targets and projectiles of different sizes striking one another as well as the effects of those collisions. The most common value used in these cases is the intrinsic collision probability P_i, defined as the likelihood that a single projectile will hit a target over a unit of time, and the mean impact velocity $V_{\rm imp}$ between the pair (e.g., Öpik 1951; Wetherill 1967; Farinella and Davis 1992; Bottke et al. 1994).

To get these values for the present-day main belt, Bottke et al. (1994) took a representative sample of main-belt asteroids (e.g., 682 asteroids with $D > 50$ km as defined by Farinellla and Davis 1992) and calculated P_i and $V_{\rm imp}$ between all possible pairs of asteroids, assuming fixed values of semimajor axis, eccentricity, and inclination (a, e, i). A common approximation made here is that the orbits can be integrated over uniform distributions of longitudes of apsides and nodes because secular precession randomizes their orbit orientations over $\sim 10^4$ year timescales. After all possible orbital intersection positions for each projectile-target pair were evaluated and weighted, they found that main belt objects striking one another have $P_i \sim 2.9 \times 10^{-18}$ km^{-2} yr^{-1} and $V_{\rm imp} \sim 5.3$ km s^{-1}. These values are fairly reasonable given what we know about the main belt population today, and comparable values can be found in many works (e.g., Farinella and Davis 1992; Vedder 1998; dell'Oro and Paolicchi 1998; Manley et al. 1998). Estimates for different portions of the main belt population striking one another have been reported as well (e.g., Levison et al. 2009; Cibulková et al. 2013).

To model collisional evolution in the primordial asteroid belt requires that certain assumptions be made about the excitation of asteroid belt bodies at that time. For example, the process that caused the main belt population to become dynamically excited (see chapter by Morbidelli et al.) should have also driven many primordial main belt asteroids onto planet-crossing orbits. While their orbits were short-lived, their higher eccentricity and inclinations would have allowed them to strafe the surviving main belt asteroids at $V_{\rm imp} > 10$ km/s for tens of Myr (e.g., Bottke et al. 2005b; Davidson et al. 2013; Marchi et al. 2013). Moreover, if the primordial main belt once had considerably more mass, as discussed in Sec. 1, these departed bodies could be responsible for a considerable amount of collisional evolution in the main belt.

A related issue is that the primordial main belt has likely been struck by sizable but transient populations on planet-crossing orbits, such as leftover planetesimals (Bottke et al. 2006; 2007), ejecta from giant impacts in the terrestrial planet region (Bottke et al. 2014), comet-like planetesimals dispersed from the primordial disk during giant planet migration (Brož et al. 2013), Jupiter-Saturn zone planetesimals pushed into the inner solar system via giant planet migration and/or evolution (Walsh et al. 2011). Most of these dramatic events are thought to take place during the first 500 Myr of Solar System history. The nature and evolution of these populations is uncertain, such that dynamical models are needed to set limits on what they were plausibly like (see chapter by Morbidelli et al.). Under certain conditions, they could also account for abundant collisional grinding in the main belt.

In all cases, dynamical models are needed to allow the

computation of P_i and $V_{\rm imp}$ between the impacting bodies and the main belt targets. From there, it is a matter of estimating the initial sizes of the populations, how fast they disperse, and how the populations undergo collisional evolution amongst themselves.

2.2 Asteroid Disruption Scaling Laws

A second key issue to modeling asteroid collisional evolution concerns the disruption scaling law. This is commonly refereed to as the critical impact specific energy $Q^*_{\rm D}$, the energy per unit target mass delivered by the projectile required for catastrophic disruption of the target (i.e., such that one-half the mass of the target body escapes). A considerable amount has been written about the value of $Q^*_{\rm D}$ (e.g., reviews in Holsapple et al. 2002; Asphaug et al. 2002; Davis et al. 2002; see also Leinhardt and Stewart 2009; 2012), and the latest on the computation of this value can be found in the chapter by Jutzi et al. For these reasons, we only briefly review the main issues here.

Using $Q^*_{\rm D}$, the diameter of a projectile $d_{\rm disrupt}$ capable of disrupting a target asteroid ($D_{\rm target}$) can be estimated as:

$$d_{\rm disrupt} = (2Q^*_{\rm D}/V^2_{\rm imp})^{1/3} D_{\rm target}, \qquad (2)$$

where $V_{\rm imp}$ is the impact velocity. We assume here that the target and projectile have the same bulk density, though that is by no means assured. Small asteroids are considered part of the "strength-scaling" regime, where the fragmentation of the target body is governed by its tensile strength, while large asteroids are considered part of the "gravity-scaling" regime, where fragmentation is controlled by the self-gravity of the target (see Sec. 4.1). Laboratory experiments and hydrocode modeling work discussed in the references above suggests the transition between the regimes occurs in the range $100 < D < 200$ m (Fig. 1).

Testing what impacts do to undamaged targets with basalt-like physical properties, Benz and Asphaug (1999) found that the the mass of the largest remnant after a collision can be fitted as a function of Q/Q^*_D, where the kinetic energy of the projectile per unit mass of the target is denoted by Q:

$$M_{LR} = \left[-\frac{1}{2} \left(\frac{Q}{Q^*_D} - 1 \right) + \frac{1}{2} \right] M_T \qquad (3)$$

for $Q < Q^*_D$ and

$$M_{LR} = \left[-0.35 \left(\frac{Q}{Q^*_D} - 1 \right) + \frac{1}{2} \right] M_T \qquad (4)$$

for $Q > Q^*_D$, where M_T is the target mass. Whenever $M_{\rm LR}$ in Eq. (3) turns out to be negative, one can assume that the target has been pulverized, such that all of its mass is lost below some minimal mass threshold.

A missing aspect of this discussion is that asteroids have wide range of physical properties and therefore may disrupt very differently than the idealized bodies used in numerical hydrocode runs. We refer the reader to the chapter by Jutzi et al., who discusses recent advances made in this area. Here we point out that all collisional models must, by necessity, make approximations to deal with complicated systems. This has led many modelers to assume that all asteroids (e.g., monoliths, rubble piles, etc.) follow the exact same $Q^*_{\rm D}$ functions for disruption. While this approach may be more accurate than one might expect (see results in chapter by Jutzi et al.), future collisional models will need to consider how specific asteroid types react to collisions.

In practice, this will mean sorting all asteroids into broad categories that can be treated by individual $Q^*_{\rm D}$ functions. One possible way to divide them up would be by spectral signatures, such as the S-, C-, and X-complexes (see chapter by DeMeo et al.). Within the complexes, bodies might share similar albedos (see chapters by Mainzer et al. and Masiero et al.), bulk densities and porosities (see chapter by Scheeres et al.), compositions, and so on. Differences between categories that could then be dealt with in a logical fashion. For example, we know that C-complex bodies often have lower bulk densities and higher porosities than S-complex bodies, and studies of primitive carbonaceous chondrite meteorites suggest many are structurally weaker and have different grain structures as well (e.g., Britt et al. 2002). Whether this affects their $Q^*_{\rm D}$ function will then need to be determined by laboratory impact experiments and numerical hydrocode simulations of asteroid collisions. There will also be the issue of how to treat the exceptional cases (e.g., the X-complex include a wide range of asteroid

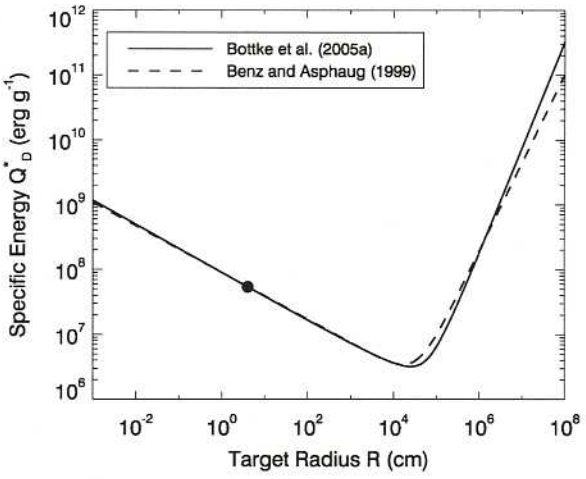

Fig. 1.— The critical impact specific energy $Q^*_{\rm D}$ defined by Benz and Asphaug (1999). This function is the energy per unit target mass delivered by the projectile that is required for catastrophic disruption of the target, such that one-half the mass of the target body escapes. The dashed line is the function derived by Bottke et al. (2005a) for their modeling results. Both functions pass through the normalization point $(Q^*_{\rm D}, D)$ set to $(1.5 \times 10^7$ erg g^{-1}, 8 cm), which was determined using laboratory impact experiments (e.g., Durda et al. 1998).

of the fragments. These equations represent empirical fits to the numerical hydrocode data. Note that comparable functions were created by Cibulková et al. (2014) from the rubble pile impact simulation results of Benavidez et al. (2012). These equations were folded into their collisional evolution models.

For fragment SFDs with very steep slopes, Eqs. (5) and (6) can easily exceed the mass of the projectile and target, which is non-physical. To avoid this problem, it is assumed that the fragment SFDs bend to shallower slopes at small sizes, though the precise diameter where this takes place is unknown and beyond the resolution limit of existing numerical hydrocode impact simulations.

It can be shown that the derived fragment SFDs from these simulations reproduce many attributes of observed asteroid families (Durda et al. 2007). With that said, however, collisional outcomes and fragment SFDs are strongly affected by gravitational forces, with the outcomes of impacts onto 400 km targets differing from those of 100 km in terms of Q/Q^*_D (P. Benavidez, personal communication). The same is probably true for smaller targets as well. Major advances in this area will therefore come from modelers who use employ fragment SFDs well suited to any possible impact outcome.

A final interesting issue here is that analytical and numerical results suggest the final equilibrium main belt SFD is often found to relatively insensitive to the details of the fragmentation law (e.g., Davis et al. 2002; O'Brien and Greenberg 2003; Bottke et al. 2005a,b; Morbidelli et al. 2009). This statement is based on experience, and it has been examined in detail. It suggests that while the fragmentation laws used are important, they are unlikely to dramatically change the equilibrium results. On the other hand, the choice of fragment SFD will be important for investigating asteroid families and transient perturbations to the main belt SFD.

2.4 Dynamical Depletion of Main Belt Asteroids by the Yarkovsky Effect

As described in the chapter by Vokrouhlický et al., $D <$ 40 km asteroids in the main belt slowly drift inward toward or outward away from the Sun in semimajor axis by Yarkovsky thermal forces. This allows some of them to reach resonances with the planets that drive them onto planet-crossing orbits, thereby allowing them to escape the main belt region altogether. Additional mobility is provided by encounters with big asteroids like Ceres and Vesta, though the net effect of this mechanism is fairly modest (e.g., Carruba et al. 2003; 2013).

The Yarkovsky effect, working in concert with resonances, therefore constitute a "sink" for small main belt asteroids. Their depletion should feed back into the collisional evolution of the main belt itself (i.e., fewer smaller bodies means fewer cratering and disruption events among larger bodies). It also means that the near-Earth object (NEO) population could be considered an short-lived component of the main belt population. This allows the NEO SFD to constrain collisional and dynamical evolution within the main belt, provided the modeler understands the translation between the main belt and NEO SFDs (e.g., Morbidelli and Vokrouhlický 2003).

The challenging part of this is to quantify the nature of small body populations lost over time via the Yarkovsky effect and resonances. Consider the following:

- Every major main belt resonance has a different character in its ability to produce long-lived NEOs (e.g., Gladman et al. 1997; Bottke et al. 2006)
- The flux of asteroids reaching dynamical resonances may change over time as a consequence of asteroid family-forming events. Large asteroid families can produce enormous numbers of fragments, while smaller ones that disrupt in strategic locations next to key "escape hatches" may also influence the planet-crossing population for some interval (Nesvorný et al. 2002a).
- The dynamical evolution of $D < 1$ km asteroids is poorly constrained because these bodies are below the observational detection limit of most surveys (e.g., Jedicke et al. 2002; see chapter by Jedicke et al.). Moreover, these bodies are also the most susceptible to YORP thermal torques that can strongly affect their drift direction and evolution (see next section).

So far, no one has yet attempted to model all of these factors and include them into an algorithm suitable for insertion into a collisional evolution code. It is a necessary but daunting task to do this correctly, given the current state of our knowledge of how the Yarkovsky/YORP effects modify the orbits, sizes, and shapes of small asteroids.

Instead, the best that has been done to date has been to generate loss rates for the asteroid belt that produce a steady state population of NEOs (Bottke et al. 2005a; Cibulková et al. 2014) (Fig. 2). This approximation can provided one with several interesting insights; for example, not including the Yarkovsky/resonance "sink" can have a substantial effect on the collisional evolution of the main belt, with more projectile left behind to disrupt larger main belt asteroids (Cibulková et al. 2014).

2.5 Asteroid Disruption by YORP Torques

The Yarkovsky-O'Keefe-Radzievskii-Paddack (YORP) effect is a thermal torque that, complemented by a torque produced by scattered sunlight, can modify the spin vectors of small asteroids (see chapter by Vokrouhlický et al.). As an asteroid obliquity evolves, its orientation can strongly affect a body's drift rate across the main belt, and therefore how quickly it reaches a resonance that can take it out of the main belt. YORP can also spin asteroids up or down. If the body has substantial unconsolidated material, or is a rubble pile, it must reconfigure itself to adjust to its new rotational

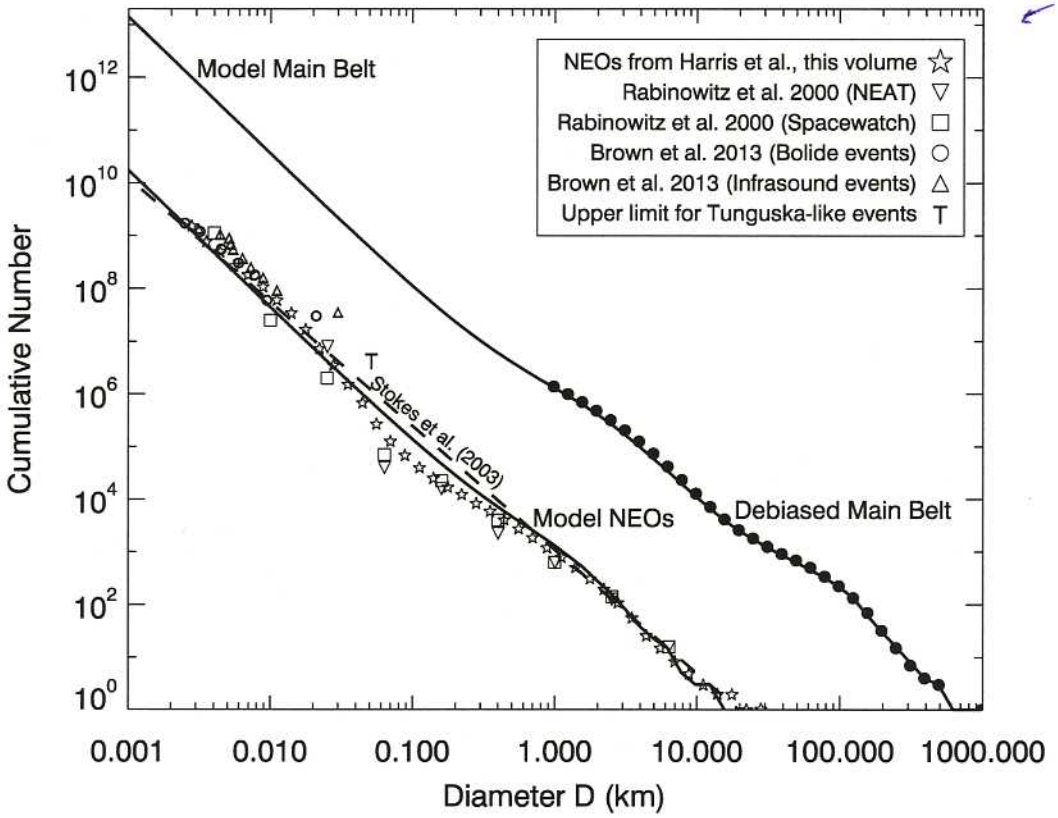

Fig. 2.— The estimated values of the present-day main belt and NEO populations according to Bottke et al. (2005b) model runs (solid lines). For reference, we plot our results against an estimate of the NEO population made by Stokes et al. (2003), who assumed the $D < 1$ km size distribution was a power-law extension of the $D > 1$ km size distribution, and a population discussed in the chapter by Harris et al. . Our model main belt population provides a good match to the observed main belt (solid black dots). Most diameter $D \lesssim 100$ km bodies are fragments (or fragments of fragments) derived from a limited number of $D \gtrsim 100$ km breakups (Bottke et al. 2005). Our NEO model population is compared to estimates derived from telescopic surveys (Rabinowitz et al. 2000) as well as satellite and infrasound detections of bolide detonations in Earth's atmosphere (Brown et al. 2014). For reference, we also include an upper limit estimate of 50 m NEOs based on the singular airblast explosion that occurred over Tunguska, Siberia in 1908. A mismatch between the NEO model and data is seen near $D \sim 0.1$ km.

angular momentum budget. In certain cases, this can cause the body to shed mass, potentially creating a satellite or an asteroid pair (see chapters by Vokrouhlický et al. and Walsh et al.).

The issue is whether YORP spin up is so efficient at causing small asteroids to shed mass that this mechanism dominates the production and elimination of bodies via collisional evolution in the same size range. This prospect is exciting, and we believe it needs to be thoroughly investigated using a wide range of models. Recent modeling work suggests YORP mass shedding effects may dominate collisions for $D < 6$ km bodies (Jacobson et al. 2014), though the model used was not subjected to the constraints discussed in Sec. 3.

A limiting factor in YORP-driven mas shedding may be our understanding of how YORP torques are affected by small topographic changes on an asteroid. For example, Statler (2009) used numerical simulations to show that minor changes in an asteroid's shape, such as the formation of a small crater or even the movement of a boulder from one place to another, could modify the YORP torques enough to change the magnitude and sign of the spin rate. This could prevent small asteroids from undergoing mass shedding as often as expected in current models (Cotto-Figueroa et al. 2013; 2014; Bottke et al. 2014). This makes this mechanism an important area for new research.

3. CONSTRAINTS ON COLLISIONAL EVOLUTION MODELS

Given the large number of "knobs" that exist in collisional evolution models, and the fact that these codes may

provide the user with non-unique solutions, it is imperative to test the results of these models against as many constraints as possible. Given the breadth of predictions for such codes, this means accounting for how individual asteroids, asteroid families, and different asteroid populations have taken on their current status. With sufficient constraints, bad parameter choices can be eliminated from contention.

On the other hand, it is important that one recognize that our understanding of main belt evolution is still limited, and the inclusion of faulty constraints into a code can also produce inaccurate results and poor predictions. Accordingly, most constraints should be treated with some caution, with the modeler and interpreter cognizant that both data and interpretation can and often do change with time.

With these caveats, we present a list of many of the constraints that should be considered when modeling the collisional evolution of the main belt.

3.1 Wavy Main Belt Size Frequency Distribution

One of the primary constraints for collision evolution models comes from the main belt SFD. Improved estimates since the review chapter of Jedicke et al. (2002) were provided by pencil beam studies of the main belt population Gladman et al. 2009), the addition of asteroids colors from the Sloan Digital Sky Survey (SDSS) (e.g., Parker et al. 2008), and new infrared data of many main belt asteroids (see chapters by Mainzer et al. and Masiero et al.). The inclusion of all of these data sets into a single debiased SFD, however, has yet to be attempted, and it is beyond the scope of this chapter.

For basic purposes, one can derive an approximate main belt SFD using the absolute magnitude H distribution provided by Jedicke et al. (2002), who combined results from the Sloan Digital Sky Survey (SDSS) for $H > 12$ (Ivezić et al. 2001) with the set of known main belt asteroids with $H < 12$. To transform the H distribution into a size distribution, one can use the relationship between asteroid diameter D, absolute magnitude H, and visual geometric albedo p_v provided by Fowler and Chillemi (1992):

$$D = \frac{1329}{\sqrt{p_v}} 10^{-H/5}. \quad (7)$$

An approximate estimate of the main belt was made by Bottke et al. (2005a), who set p_v to 0.092 in order to match the observed asteroids described cited in Farinella and Davis (1992). This population is shown in Fig. 2. Overall, the observed and debiased main belt SFD is wavy, with "bumps" near $D \sim 3$ km and one near $D \sim 100$ km. The reason for these bumps will be discussed in Sec. 4.

For more precise constraints, and more model variables, one can treat different regions of the main belt separately. For example, Cibulková et al. (2014) divided the main belt population into six distinct components: inner, middle, pristine, outer, Cybele, and high inclination regions. This allowed them to track how each different regional SFDs evolved in response to various collisional and dynamical processes. The observed SFDs in each region, however, have yet to be debiased, which means they must be treated as lower limits for modeling constraints.

3.2 Asteroid Families

Asteroid families provide another powerful way to constrain asteroid collisional models. As discussed in the chapter by Nesvorny et al., these remnants of cratering and catastophic disruption events are identified in the main belt by their clustered values of proper semimajor axes $a_{\rm p}$, eccentricities $e_{\rm p}$, and inclinations $i_{\rm p}$. The problem using them to test our model runs is that estimates of ancient family ages can be imprecise and small families can also be eliminated over time by collisional and dynamical processes.

For this reason, the best starting constraints come from families where the parent body was large enough that their fragments could not be erased over 4 Gy of evolution. We assume families formed prior to 4 Gyr ago were erased by sweeping resonances produced by late giant planet migration (see chapter by Morbidelli et al.). Using results discussed in Durda et al. (2007) (see also Cibulková et al. 2014), there are approximately 20 observed families created by catastrophic disruptions of parent bodies with sizes $D_{\rm PB} > 100$ km , where the ratio of the largest fragment's mass to the parent body mass is $M_{\rm LR}/M_{\rm PB} < 0.5$ (Fig. 3).

It is also useful to use the distribution of family parent body sizes to compare model to data. In one case, Bottke et al. (2005a,b) used results later published in Durda et al. (2007) to argue that the number of families formed over the last 3.5 Gy from catastrophic breakups of parent bodies whose sizes were within incremental bins centered on diameters $D = 123.5, 155.5, 195.7, 246.4, 310.2$, and 390.5 km were 5, 5, 5, 1, 1, 1, respectively. New family identifications discussed in the chapter by Nesvorny et al. can be used to update these values.

Ideally, a good collisional model must account for all types of collisions, even relatively small cratering events. For the purpose of comparison with observations, one has to carefully select synthetic events which would still be observable. Even though this number ($N_{\rm fam} \sim 20$) appears well defined above, it is difficult to assess its uncertainty for the following reasons:

- Determining the size of the parent of an asteroid family depends on the observed fragment distribution, which has experienced collisional and dynamical evolution, and the nature of the precise breakup involved, which may be uncertain. The existence of interlopers within the family can also be hard to exclude.
- There are overlapping families that are difficult to separate unambiguously (e.g. several families exist in the Nysa/Polana region; M. Dykhuis, personal communication);

- The method used for the parent-body size determination in Durda et al. (2007) may exhibit some systematic issues since it involves a number of assumptions.

Taken together, the uncertainty of $N_{\rm fam}$ is at least the order of a few, if not more.

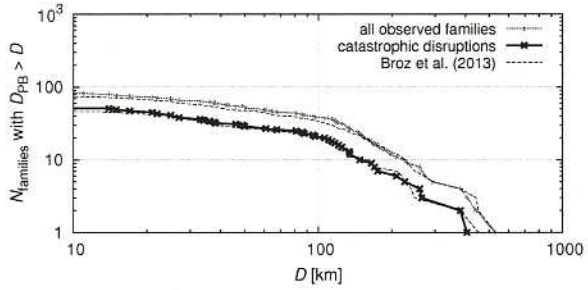

Fig. 3.— A production function (i.e. the cumulative number $N(>D)$ of families with parent-body size $D_{\rm PB}$ larger than D) for all observed families (gray) and families corresponding to catastrophic disruptions (black), i.e. with largest remnant/parent body mass ratio lower than 0.5. Adapted from Brož et al. (2013) and updated according to Nesvorný et al. (this volume). The families were assumed to form prior to 4 Gyr ago, with earlier ones dispersed by sweeping resonances produced by late giant planet migration (see chapter by Morbidelli et al.).

The distribution of the dynamical ages and sizes of families, as derived using the methods discussed in the chapter by Nesvorný et al. , may also provide another metric to estimate family completeness. For example, Fig. 4 shows estimates of the ages of cratering and catastrophic disruption events for families derived from different parent body sizes (Brož et al. 2013). We caution the reader that discerning these values for heavily evolved ancient families is problematic, and large uncertainties exist. We therefore use Fig. 4 as a guide to glean insights into interesting possibilities, not as the last word on this topic.

We focus here on asteroid families whose parent bodies diameters $D_{\rm PB} > 100$ km; they are presumably more difficult to eliminate by collisional and dynamical processes. For families formed over the last 2 Gyr, we find several with $100 < D_{\rm PB} < 200$ km and few with $D_{\rm PB} > 200$ km. The opposite is found for families older than 2 Gyr; only a few $100 < D_{\rm PB} < 200$ km families exist, while several $D_{\rm PB} > 200$ km are found.

The difference between the two sets warrants additional study, but we lack sufficient data to state they are highly unusual. The probability that two $D_{\rm PB} > 200$ km families formed in the last 2 Gyr out of the seven identified with ages < 4 Gyr is 23%. The number of $100 < D_{\rm PB} < 200$ km families that formed at different times are also not unusual from a statistical standpoint. Overall, there are also approximately the same number of young ($t_{\rm age} < 2$ Gyr) and old (> 2 Gyr) families produced by the catastrophic disruptions of $D_{\rm PB} > 100$ km bodies.

The most intriguing issue here is that there are no identified $D_{\rm PB} < 100$ km families that are > 2 Gyr old. This hints at the possibility that some $100 < D_{\rm PB} < 200$ km older than 2 Gyr are so evolved that they escaped detection. If true, one could argue that something interesting was going on that was producing $D_{\rm PB} > 100$ km families in the billion years or so after the completion of the major dynamical depletion events > 4 Gyr (see Sec. 1 and the chapter by Morbidelli et al.).

Along these lines, one way to account for the unusual distribution of families in Fig. 4 is to assume that some small families are actually remnants, or "ghosts", of much larger older families. A possible example might be the cluster of asteroids near asteroid (918) Itha (Brož et al. 2013). It exhibits a very shallow SFD, which could be a possible outcome of comminution and dynamical evolution by the size-dependent Yarkovsky effect. An excellent place to look for ghost families would be the narrow portion of the main belt with semimajor axis a between 2.835-2.955 AU. This pristine zone, which is bounded by the 5:2 and 7:3 mean-motion resonances with Jupiter, has a limited background population of small asteroids. We postulate it could resemble what the primordial main belt looked like prior to the creation of many big families.

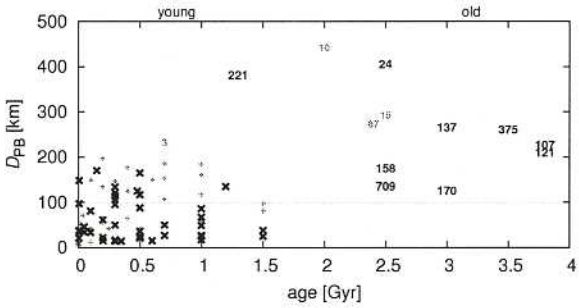

Fig. 4.— The relation between dynamical ages of families and the sizes of their parent bodies. Black labels correspond to catastrophic disruptions, while cratering events are labeled in gray. Some of the families are denoted by the designation of the largest member. Adapted from Brož et al. (2013) and updated according to Nesvorný et al. (this volume).

An independent calibration of collisional models might also be based on very young families, namely younger (and larger) than some carefully estimated upper limit for which the respective sample is complete. Indeed, there are many examples of young families with well-determined ages: Veritas (8.3 ± 0.5) Myr (Nesvorný et al. 2003), Karin (5.8 ± 0.2) Myr (Nesvorný and Bottke 2004), Lorre (1.9 ± 0.3) Myr (Novaković et al. 2012), P/2012 F5 (Gibbs) (1.5 ± 0.1) Myr (Novaković et al. 2014), etc. A collisional model then would have to reproduce the number of these events in the last say $\simeq 10$ Myr of the simulation.

3.3 Impact Basins on (4) Vesta

(4) Vesta is one of the most singular asteroids in the main belt. Not only is it among the largest asteroids, with a diameter of 525 km, but it is also has a largely intact basaltic

crust that was put in place shortly after it differentiated some 2-3 Myr after CAIs (see chapter by Russell et al.). We do not consider the impact record on Vesta prior to or during the formation of this crust, though Vesta's abundance of highly siderophile elements may eventually allow us to infer what happened during this ancient period (e.g., Dale et al. 2012). Decades of ground-based observations, combined with the in situ observations of Vesta by the Dawn spacecraft, have shown that the spectral signatures found in Vesta's crust are a good match to the eucrites, howardites, and diogenite meteorite classes (see chapter by Russell et al.).

Vesta also has two enormous basins that dominate its southern hemisphere: Rheasilvia, a 505 km diameter crater with an estimated crater retention age of 1 Gyr, and Veneneia, a 395 km crater with a crater retention age of > 2 Gyr (Marchi et al. 2012). Rheasilvia, being younger, overlaps with and has largely obscured Veneneia (Schenk et al. 2012). The formation of each basin is also thought to have produced a set of fracture-like troughs, or graben, near Vesta's equator (Buczkowski et al. 2012). Studies of each trough group show they form planes that are orthogonal to the basin centers. Recent simulations of the formation of the Veneneia and Rhealsilvia basins using numerical hydrocodes suggest they were created by the impact of 60-70 km diameter projectiles hitting Vesta near 5 km/s (Jutzi et al. 2013). These same events likely produced the majority of the observed Vesta family, a spread out swarm of $D < 10$ km asteroids in the inner main belt with inclinations and spectral properties similar to Vesta itself (see chapter by Scott et al.).

Vesta shows no obvious signs that basins similar in size to Rheasilvia or Veneneia were ever erased or buried after its basaltic crust was emplaced; nothing notable is detected in Vesta's topography, and there are no unaccounted sets of troughs that could be linked with a missing or erased basin. This means Vesta is probably complete in Rheasilvia- or Veneneia-sized basins. This constrains both the size of many primordial populations as well as how long they could have lasted on Vesta-crossing orbits (e.g., main belt asteroids, leftovers planetesimals from terrestrial and giant planet formation, the putative late heavy bombardment population, Jupiter-family comets, etc.).

As a worked example, consider that if we use the main belt asteroid population described in Bottke et al. (1994), where there are 682 main belt asteroids with $D > 50$ km, we find that the probability that Vesta has 0, 1, 2, or 3+ Rheasilvia/Veneneia formation events over the last 4 Gyr is 50%, 35%, 12%, and 3%, respectively. If Rheasilvia and Veneneia are actually both < 2 Gyr old, however, these values change to 70%, 25%, 4%, and 0.5%, respectively. The 4% probability for the observed situation is surprisingly small, and it suggests two possibilities: Veneneia's crater retention age was strongly affected by the Rheasilvia formation event, and its formation age is older than its crater retention age (Marchi et al. 2012), or the basins on Vesta's surface beat the odds. Note that testing modestly smaller projectiles to make the basins, such as $D > 35$ km asteroids (Asphaug et al. 1997), only increases the probabilities above by a factor of 2 or so.

These calculations become even more interesting if we assume the main belt population was larger in its early history, and/or that it was hit by objects from outside the main belt (see chapter by Morbidelli et al.). Bottke et al. (2005a) argued the main belt experienced the equivalent of $\sim$ 7.5-9.5 Gyr of collisional evolution over the last 4.56 Gyr (i.e., roughly translated as the number of impacts Vesta would get if it resided in the current main belt population for this time; see Sec. 4). For simplicity, we round this value to 10 Gyr, which makes the probability of getting 0, 1, 2, or 3+ basins at any time in Vesta's history 17%, 30%, 27%, and 20%, respectively. This would place Rheasilvia/Veneneia combination near the center of the probability distribution. If Rheasilvia/Veneneia formed < 2 Gyr ago, however, we not only have to explain their existence, but also the absence of ancient basins; large primordial populations are more likely to create ancient basins than young ones. The probability of these events taking place is only $\sim 1\%$.

Therefore, from a purely statistical point of view, one could argue that the main belt was probably more massive in the past, and that Veneneia's minimum age of ~ 2 Gyr is not its formation age. An older age for Veneneia would also allow it to be the source for numerous Vesta family members with low inclinations, which need billions of years to reach these orbits via Yarkovsky drift and resonances (Nesvorný et al. 2008). Further work will be needed to see if the "facts on the ground" confirm or reject these predictions.

3.4 Near-Earth Asteroids, Asteroid Craters, and Lunar Craters

Asteroids in the main belt have struck other asteroids for the age of the Solar System. This means that projectile SFDs ranging from a few meters to multi-km sizes can be constrained over hundreds of millions to billions of years by craters found on asteroids imaged by spacecraft missions (see chapter by Marchi et al.). The main belt SFD also produces planet-crossing asteroids via the combined Yarkovsky/YORP effects (see Vokrouhlicky et al.). This means that the observed planet-crossing asteroid population can also be used to provide main belt SFD constraints. We focus here on the best understood component of the population, namely the NEAs (see chapter by Harris et al.) Finally, Earth-crossing asteroids in the NEA population have slammed into the Earth and Moon over billions of years, which means the crater SFDs and impact byproducts on these worlds can help us determine how the main belt SFD have evolved over these times.

The key issue for all these data is interpretation; the ages and SFDs of cratered terrains are often uncertain or complicated, and short-term changes in the flux or shape of impacting SFDs can be hard to decipher amid the integrated histories of cratered surfaces. For this reason, a full discussion of all cratering issues is beyond the scope of this section.

Stöffler and Ryder 2001; Morbidelli et al. 2012). Given that this flux is fed by the main belt population, changes in the lunar impactor flux over time should correspond at some level to what took place in particular regions of the main belt.

Studies of small lunar craters ($D < 1$ km) on specific Copernican and Eratosthenian-era terrains suggest the impact flux of very small impactors has been fairly constant, within a factor of 2 or so, for the last 3.2 Gyr (e.g., Hiesinger et al. 2012, but see also Robbins 2014). For reference, the ages of the former era are often considered to be roughly 1 Gyr old, while those of the latter are defined by the ages of samples returned by the Apollo 12 astronauts (Stöffler and Ryder 2001). This implies the main belt population in the inner and central main belt feeding $D < 0.05$ km bodies to resonances was also reasonably stable as well.

For larger impactors, the lunar data is more difficult to interpret, though it also hints at a steady state flux. For example, the best available crater SFD of the largest Copernican- and Copernican and Eratosthenian-era craters on the Moon are shown in Fig. 6 (McEwen et al. 1997; Ivanov et al. 2002). The Copernican and Eratosthenian-era craters are roughly a factor of 3 higher than the Copernican-era craters. If the ages of these eras suggested above are reasonable, these data would indicate there have been a fairly steady supply of kilometer-sized main belt asteroids to the NEA population and the Moon over 3 Gyr, at least within a factor of 2.

We caution that this interpretation may be subject to revision in the near future once data from the Lunar Reconnaissance Orbiter has been fully evaluated (e.g., Kirchoff et al. 2013; Robbins 2014). For example, asteroid family-forming events in strategic locations could potentially affect the lunar impact flux for some period of time (Nesvorný et al. 2002). Given our present-state of knowledge, however, it is fair to say that deviations from a steady state over long time spans may be modest for most projectile sizes.

There are two main reasons these results are of critical importance for collision models:

1. Collisional models of the main belt and NEA SFD need to achieve a quasi-steady state for the last several billions of years (or have an alternative way to explain the above constraints). This likely rules out scenarios where a very large main belt SFDs is ground down over billions of years of comminution, with the observed SFD only achieved near the present time (see Davis et al. 2002). Such models should produce strongly-decaying lunar impact fluxes over the last 3 Gyr, and they are not observed.

2. A steady state main belt SFD allows modelers to predict the ages of asteroids surfaces with reasonable accuracy, though caution should still be employed (see chapter by Marchi et al.).

3.5 Main Belt Binaries Formed by Impacts

The population of certain types of asteroid binaries may also constrain the collisional evolution of the main belt. Using numerical hydrocode simulations to model asteroid impacts on $D = 100$ km target bodies, Durda et al. (2004) found that large-scale cratering events can create fragments whose trajectories can be changed by particle-particle interactions and by the reaccretion of material onto the remnant target body. Under the right circumstances, impact debris can enter into orbit around the remnant target body, which is a gravitationally reaccreted rubble pile, to form a SMAshed Target Satellite (SMATS).

We expect SMATS to be rather isolated in space; while their formation events produce asteroid families dominated by small fragments, most of these bodies are readily removed or dispersed by collisional and dynamical evolution. As of a few years ago, detection limits of ground-based adaptive optics searches limited the discovery of SMATS to primary to- secondary diameter ratios smaller than 25 (e.g., Merline et al., 2002). This population is thought to be complete, so we focus on these binaries here. In a survey of 300 large main belt asteroids, Merline et al. (2002) reported that four $D > 140$ km bodies that had relatively large satellites (i.e., $D > 10$ km) that were not in asteroid families produced by catastrophic disruption events: (22) Kalliope, (45) Eugenia, (87) Sylvia, and (762) Pulcova. Durda et al. (2004) classifies SMATS made by catastrophic collisions in a different manner.

Additions since that time to the SMATS record could include (216) Kleopatra and (283) Emma, whose primaries have diameters that are nearly 140 km. The secondary sizes of Eugenia and Emma, however, are very close to our primary-to-secondary diameter ratio limit, and Kleopatra appears to have an iron rather than stony composition, such that the results of Durda et al. (2004) may not be applicable. This leaves the net value somewhere in the range of 3-6. The binary (90) Antiope is excluded here because it is a likely byproduct of the catastrophic disruption that produced the Themis family.

Using their runs, Durda et al. (2004) estimated that the expected frequency of SMATS-forming events by non-catastrophic collisions in the present-day main belt was $f = 0.9\text{-}1.7 \times 10^{-11}$ yr^{-1}. If one then assumes that the current population of $D > 140$ km bodies, $N = 94$, is similar to that from 4 Gyr ago, we would expect these production rates to yield 3-6 SMATs on average. These results are an excellent match to the 3-6 SMATs discussed above.

These results place upper limits on what happened during the primordial phase of the asteroid belt, depending on the planet formation evolution model invoked. For example, as described in the chapter by Morbidelli et al., the main belt potentially had an early massive phase, where numerous SMATS should have been made. A dynamical depletion event at the end of this phase would then remove most of the excess mass as well as most of the newly-formed SMATS. Effectively, this would make the remnant number of primordial SMATS the product of f, N, and the time interval that the excess population existed in the main belt. For Nice

model simulations (see chapter by Morbidelli et al.), where the main belt is only a few times more massive than the current population for $\sim$ 0.5 Gyr, this would yield $\sim$ 1 extra SMAT on average, not enough to affect the results above.

On the other hand, SMATS provide powerful constraints against evolution scenarios where collision grinding alone removes most of the primordial mass of the main belt. This scenario is already problematic, as discussed above, but numerous collisions may produce a net amount of SMATS that exceeds observations. Similarly, some have invoked massive planetesimal populations on terrestrial planet-crossing orbits, and no Nice model, as a way to explain the cratered surfaces and various properties of the Moon and other worlds (e.g., Ćuk et al. 2012). Many of the small bodies, however, should evolve onto main belt-crossing orbits, where their collisions should create numerous SMATS. Given that we see little evidence for an abundance of primordial SMATS, these models can potentially be tested on this basis.

3.6 Asteroid Spin Rates and Spin States

Asteroid spin rates are affected by collisions, so it is plausible they can be used as constraints on main belt evolution. A problem with this is that many $D > 50$-100 km bodies may still have spins that were largely put in place by the planetesimal accretion process. A review of the spin rate literature for the largest asteroids can be found in Bottke et al. (2005a). For smaller bodies, the spin rates and obliquities of $D < 30$-40 km asteroids are likely dominated by the effects of YORP thermal torques (e.g., Pravec et al. 2002; see chapter by Vokroulicky et al.). Given this, an unambiguous signal of collisions affecting spin vectors in the main belt may be limited to bodies whose evolutionary context is well understood.

The interested reader can consider the spin evolution models of Farinella et al. (1992) and Marzari et al. (2011) for their views on this topic. They should also examine results from the numerical hydrocode simulations of Love and Ahrens (1997), who argued that small erosive collisions have a minimal effect on an object's spin, while catastrophic disruption events essentially destroy all "memory" of the target body's initial spin. The collisional signal we are looking, therefore, may be limited to specific remnants of certain family-forming events.

An alternative way to obtain a model constraint may be found in the spin vectors of asteroids in the Koronis asteroid family. The Koronis family is thought to be one the asteroid belt's most ancient families, with an estimate age of 2-3 Gy (see chapter by Nesvorný et al.). After years of painstaking observations of Koronis family members, including 21 of the 25 brightest Koronis family members, Slivan et al. (2003; 2009) and Slivan and Molnar (2012) reported that nearly all of the observed 15-40 km diameter Koronis family members with prograde spins have clustered spin periods between 7.5-9.5 h and spin obliquities between 39-56°. Those with retrograde spins have obliquities larger than 140° nearly with periods either < 5 h or > 13 h. Vokrouhlicky et al. (2003) demonstrated that all of these spin states were a byproduct of YORP thermal torques. The prograde cluster was created by an interaction between YORP torques and spin orbit resonances, and are now called "Slivan states".

The predicted timescales for these objects to reach these spin states is several billions of years. During that time, collisions did not strongly affect their spin periods or their obliquities; if they had, we would see at least a few bodies with random spin vector values. Limits on this come from (243) Ida, a member of the prograde cluster with dimensions of $53.6 \times 24.0 \times 15.2$ km; it was apparently unaffected by the formation of two $\sim$ 10 km diameter craters formed on its surface.

Statistically, we would expect catastrophic disruptions to be more rare than smaller, less energetic impact events that can modify an asteroid's spin state. In the ancient Koronis family, however, the spin vectors of many large objects show no evidence that collisions have affected them. This presents a key challenge to collisional models that assume disruption events among 20-40 km bodies are relatively common; can this outcome be reconciled with the spin states of Koronis family members? A similar argument could potentially be developed regarding the anisotropic obliquities found among $D < 30$ km asteroids residing in the background main belt population (e.g., Hanuš et al. 2013).

3.7 Additional Constraints

The constraints discussed above are far from complete, and many other data sets could be brought to bear in a collisional model. For example, constraints not discussed include (i) the cosmic ray exposure ages of stony meteorites (e.g., Eugster 2003), (ii) the orbital distribution of fireballs (e.g., Morbidelli and Gladman 1998), (iii) the population of V-type asteroids across the main belt (see chapter by Scott et al.), (iv) the crater records found on Mercury, Venus, Earth, and Mars (e.g., Ivanov et al. 2002), (v) all asteroid families not discussed here (see chapter by Nesvorný et al.), (vi) the shock degassing ages of meteorites (e.g., Marchi et al. 2013), and so on. We consider this to be one of the richest and most fascinating problems in asteroid science, and it allows us to take advantage of what we have learned about asteroids and meteorites from nearly every discipline.

4. INSIGHTS FROM MODELING RESULTS

Existing collisional modeling work has provided us with insights into the nature of planetesimal formation, asteroid fragmentation and evolution, planet formation processes, and the bombardment history of the inner solar system. Here we summarize some of those findings.

4.1 ~~Interpreting the Shape of the Main Belt~~ Size Frequency Distribution

The bump in the main belt SFD near $D \sim$ 2-3 km (Fig. 2) is a byproduct of collisional evolution (Campo Bagatin et al. 1994; see Davis et al. 2002), and as we will show, it is driven by a change in the Q_D^* function near $D \sim 0.1$ km. To trace its origin, we start with the classic work of Dohnanyi (1969), who analytically modeled collisions among a SFD of self-similar bodies and found the steady state SFD should follow a differential power law with an exponent of -3.5. Dohnanyi assumed that the strength per unit mass of the colliding bodies is independent of size. In reality, though, for bodies smaller than ~1 km in diameter, material properties cause strength to decrease with increasing size, while for larger bodies, self-gravity makes it more difficult to shatter a body and disperse its fragments, leading to an increase in strength with increasing size (e.g., Asphaug et al. 2002; Holsapple et al. 2002; Davis et al. 2002). This provides us with the classic Q_D^* function discussed above.

The dependence of the power-law index of the size distribution on these parameters was explored analytically by O'Brien and Greenberg (2003), and we repeat the main results here. First consider the steady-state of a colliding population of bodies whose strength is described by a single power law. The population is described by the power law:

$$\mathrm{d}N = BD^{-p}\mathrm{d}D \tag{8}$$

where $\mathrm{d}N$ is the incremental number of bodies in the interval $(D, D+\mathrm{d}D)$. While B should technically be negative as there are more small bodies than large bodies, it is defined to be positive here to avoid physically unrealistic result of having negative numbers of bodies in a given size interval. p is the power-law index of the population. Eq. (8) would plot as a line with a slope of $\sim p$ on a log-log plot.

O'Brien and Greenberg (2003) considered the case where the impact strength Q_D^* is given by a power law

$$Q_D^* = Q_o D^s, \tag{9}$$

where Q_0 is a normalization constant and s is the slope of Eq. (9) on a log-log plot. They find that, in collisional equilibrium, the power-law index p in Eq. (8) is given by

$$p = \frac{7 + s/3}{2 + s/3}. \tag{10}$$

For $s = 0$, which corresponds to size-independent strength Q_D^*, this gives the classical Dohnanyi steady-state solution of $p = 3.5$. For the more realistic case where Q_D^* decreases with increasing size for small bodies and increases for larger bodies once gravity becomes important (as schematically shown in Fig. 7), O'Brien and Greenberg (2003) show that the strength- and gravity-scaled portions of the size distribution have power-law indices that are only dependent on the slope of Q_D^* in the strength- and gravity-scaled regimes, respectively. The power-law index of the size distribution in the strength-scaled regime p_s has no dependence on the slope s_g of Q_D^* in the gravity-scaled regime, and vice versa; p_s is found by using s_s, and p_g is found by using s_g. Because s_s is usually negative and s_g is usually positive, Eq. 10 yields $p_s > 3.5$ and $p_g < 3.5$.

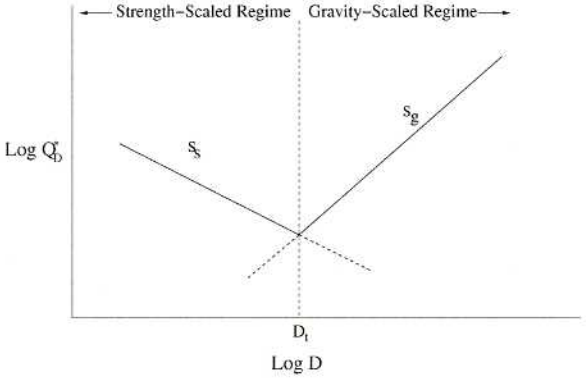

Fig. 7.— A schematic Q_D^* law for a population with different strength properties for large and small bodies. Q_D^* consists of two different power laws with slopes s_s and s_g joined at the transition diameter D_t. In the strength-scaled regime, material properties control the effective strength, while in the gravity-scaled regime, gravity dominates the effective strength through self-compression and gravitational reaccumulation of collisional fragments.

While the general slope of the size distribution in the gravity regime is unaffected by Q_D^* in the strength regime, the transition in slope of the size distribution will lead to waves that propagate through the size distribution in the gravity regime. In the derivation of p_g, it is implicitly assumed that all asteroids were disrupted by projectiles whose numbers were described by the same power law. However, for those targets just larger than the transition diameter D_t between the strength- and gravity-scaled regimes (i.e. near the small end of the gravity-scaled regime), projectiles are mostly smaller than D_t, and hence are governed by the strength-scaled size distribution.

Consider the two steady-state power laws describing the population in the strength- and gravity-scaled regimes, joined at the transition diameter D_t as shown in Fig. 8, and let $D_{t,dis}$ be the diameter of the body which can disrupt a body of diameter D_t. Due to the transition from the gravity-scaled regime to the strength-scaled regime below D_t, bodies of diameter $D_{t,dis}$ are more numerous than would be expected by assuming that all bodies are gravity scaled, leading to a configuration that is not in a steady state. A steady-state configuration can be achieved by "sliding" the population in the strength-scaled regime down in number, as shown in Fig. 8. The shift in number of bodies at D_t does not result in a simple discontinuity as shown in Fig. 8, but instead causes perturbations to the size distribution in the gravity-scaled regime ($D > D_t$). The underabundance $\Delta \mathrm{Log}N(D_t)$ of bodies of diameter D_t (a 'valley') leads to an overabundance of bodies which impactors of diameter D_t are capable of destroying (a 'peak'), which in turn leads to another 'valley' and so on. This results in a wave of

amplitude $|\Delta \mathrm{Log} N(D_t)|$ that propagates through the large body size distribution as shown in Fig. 8. The average power-law index p_g of the population in the gravity-scaled regime will not be significantly changed by the initiation of this wave; the wave oscillates about a power law of slope p_g.

This analysis allows O'Brien and Greenberg (2003) to derive analytical expressions for the amplitude of the waves, as well as the approximate positions of the 'peaks' and 'valleys' in the size distribution.

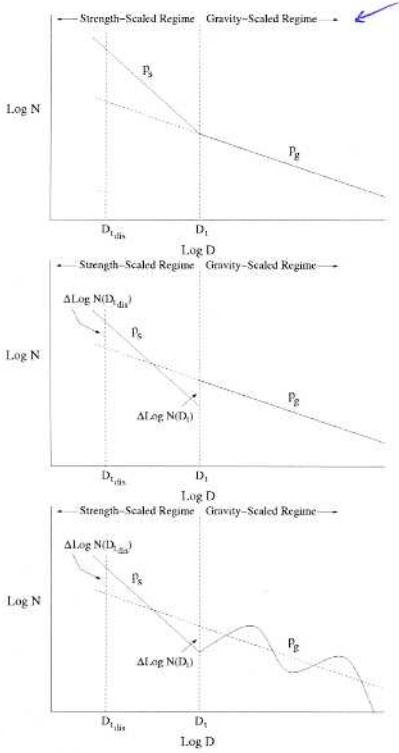

Fig. 8.— Sequence showing how waves form in the SFD as a result of a change in strength properties at D_t. (a) For a Q_D^* law such as that shown in Fig. 7, the resulting steady-state population is steeper for smaller, strength-scaled bodies (population index p_s) than for larger, gravity-scaled bodies (population index p_g). Thus, impactors capable of destroying bodies of diameter D_t are overabundant relative to what would be expected by extrapolating the gravity regime slope. This configuration is not in collisional equilibrium. (b) To counteract this, the number of bodies of diameter D_t and smaller decreases by a factor $\Delta \mathrm{Log} N(D_t)$ so that there are fewer 'targets' of diameter D_t and fewer impactors of diameter $D_{t_{dis}}$. (c) The decrease in bodies of diameter D_t leads to an overabundance of bodies which can be destroyed by impactors of diameter D_t, which in turn leads to a depletion of larger bodies and so on. Thus, a wave is formed in the large-body population.

The waves will not continue on to larger bodies if they have long collisonal lifetimes. The origin of the bump for $D > 100$ km bodies is discussed in the next section.

4.2 Large Asteroids as Byproducts of Planetesimal Formation

One of the most difficult issues to deal with concerning main belt evolution is estimating the initial SFD created by planetesimal formation mechanisms. Given the current uncertainties surrounding planet formation, a enormous range of starting SFDs are theoretically plausible. This has caused many groups to winnow these possibilities down using collisional models.

For example, Bottke et al. (2005a,b) tested a wide range of initial SFDs and Q_D^* functions to determine which combinations work the best at reproducing the observational constraints discussed in Sec. 3. They found that Q_D^* functions similar to those derived in numerical SPH experiments of asteroid breakup events (Benz and Asphaug 1999) tended to work the best (Fig. 1), though this made their $D > 100$ km asteroids very difficult to disrupt. Accordingly, they inferred that the shape of the main belt SFD for $D > 100$ km asteroids was probably close to its primordial shape (Fig. 2). Interestingly, this prediction is consistent with several pioneering papers from the 1950's and 1960's (Kuiper et al. 1958; Anders 1965; Hartmann and Hartmann 1968).

Next, they tested initial main belt SFDs where the incremental power law slope of -4.5 between $100 < D < 200$ km had been extended to $D < 100$ km bodies (Fig. 9). This eliminated the observed bump near $D \sim 100$ km. They found bodies in this size range were so difficult to disrupt that initial SFDs with these shapes could not reproduce constraints. They argued from this that the bump near 100 km in the main belt SFD is primordial and that $D < 100$ km bodies probably had a shallow power law slope. Accordingly, this would indicate the planetesimal formation process favors the creation of bodies near 100 km (or larger), with smaller bodies increasingly fragments produced by the disruption of large asteroids. These results may act as a guide for those studying planetesimal formation processes (e.g., Morbidelli et al. 2009; see chapter by Johansen et al.).

4.3 Collisional Evolution of the Primordial Main Belt

To understand the history of the main belt, it is important to quantify how much collisional evolution has taken place their over its history. This means choosing a starting SFD and then evaluating what it takes to reach its present-day state. The problem is there are many different ways to get from start to finish, and the available constraints may be insufficient to tell us which pathways are favored.

In order to glean insights into this, one can adopt a simplistic but useful metric that can help us evaluate what different evolutionary paths might do. First, let us assume that the main belt is roughly self-contained in terms of collisions, such that we can largely ignore impacts from external

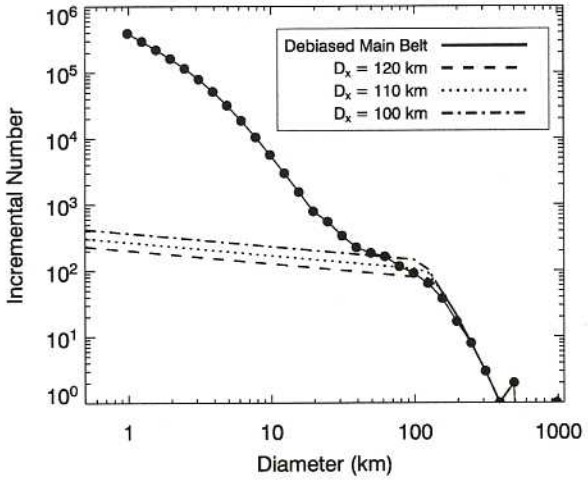

Fig. 9.— The debiased main belt size frequency distribution as defined in the main text (solid line). The dashed curves show possible initial shapes of the primordial main belt SFD (Bottke et al. 2005a). They found a best fit in their runs for an elbow near $D \sim 110$-120 km. It is likely the primordial population was larger that the SFDs shown here, with most of the mass eliminated by dynamical processes.

sources like escaped main belt asteroids, leftover planetesimals, comets, etc. Second, we assume the intrinsic collision probabilities and impact velocities of main belt asteroids hitting one another has remained unchanged over its history. Third, we assume the main belt's SFD has been close to its current shape throughout its history, though it may have been larger in the past. We define this size to be a factor f, the ratio of the main belt's SFD during some past interval of time defined as ΔT over the present-day main belt SFD. Together, these values allow us to estimate the degree of collisional evolution experienced by the main belt in terms of the time exposed to different population sizes.

This metric allows to play with evolution scenarios. The simplest example is the nominal case where the current main belt SFD ($f = 1$) undergoes collisional evolution over its lifetime ($\Delta T = 4.56$ Gyr). The two values multiplied together yield 4.56 Gyr of collisional grinding. In a more complicated example, lets assume a dynamically excited primordial main belt had $f = 300$ for 3 Myr (0.003 Gyr). At that point, most of the population was lost via escaping embryos or a migrating Jupiter, which reduced it to $f \sim 5$ for ~ 0.5 Gyr. Then, at ~ 4 Gyr, 80% of the bodies were lost via sweeping resonances driven by late giant planet migration, which left the surviving population close to its current state ($f = 1$) for the next ~ 4 Gyr. Taking all of the multiples, one can say that collectively the survivors experienced $(0.9 + 2.5 + 4) = 7.4$ Gyr of collisional evolution. This pseudo-time tells us that this main belt roughly experienced the collisional evolution equivalent of a $f = 1$ main belt going through 7.4 Gyr of comminution.

Using a collisional model that took advantage of these concepts, as well as the constraints above, Bottke et al. (2005a) found median pseudo-times of 7.5-9.5 Gyr for their best fit runs, with error bars of a few Myr on each end of this range. An example of one of their runs is shown in Fig. 10. Their interpretation was that main belt SFDs obtained its wavy shape by going through an early time interval where the main belt survivors were exposed to many more projectiles than are observed today, with most of those bodies due lost to dynamical processes. Thus, the wavy main belt SFD could be considered a "fossil" produced in part by early collisional evolution in the primordial main belt.

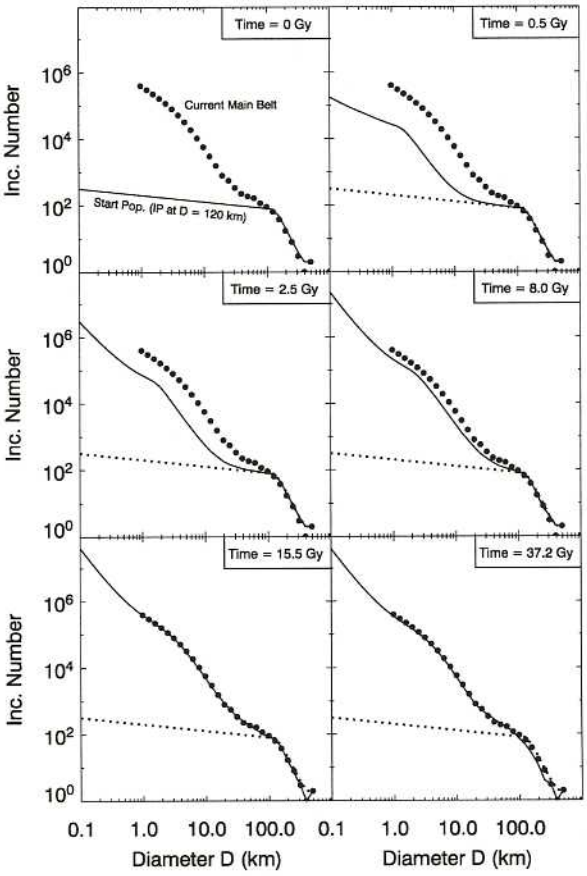

Fig. 10.— Six snapshots from a representative run where Bottke et al. (2005a) tracked the collisional evolution of the main belt size distribution for a pseudo-time of 50 Gy. This run uses a starting population with $D_x = 120$ km. The bump near $D \sim 120$ km is a leftover from accretion, while the bump at smaller sizes is driven by the transition at $D \sim 0.2$ km between strength and gravity-scaling regimes in $Q^*_{\rm D}$. The model main belt achieves the same approximate shape as the observed population at $t_{\rm pseudo} = 9.25$ Gy (not shown). The model closely adheres to the observed population for many Gy after this time. Eventually, comminution eliminates enough $D > 200$ km bodies that the model diverges from the observed population.

This pseudo-time range above can be used to explore dynamical evolution scenarios, particularly those that create abundant main belt populations. For example, using our simple metric, one could replace the middle component, which roughly corresponds to the the "Jumping Jupiter" version of the Nice model (Morbidelli et al. 2010; Marchi et al. 2013), with the original Nice model where $f \sim 20$ for ~ 0.5 Gyr (Gomes et al. 2005). This change yields $(0.9 + 10 + 4) = 14.9$ Gyr, a pseudo-time outside the favored range. While it cannot be ruled out statistically, it does suggest that collisional evolution needs to be explored in greater depth here.

Another interesting property of Fig. 10 is that once it achieve the present-day shape of the main belt SFD, it tends to keep it for an extended time. This would explain why the main belt SFD could remained in a near steady state condition for billions of years. While it would constantly changing and losing bodies by collisional, dynamical, and YORP spin up processes, it would also be steadily replenished by new large breakup events. This means the vast majority of disruption events produce too few fragments to push the main belt SFD out of equilibrium for very long. This result also explains why the non-saturated crater populations on Gaspra, Vesta (i.e., the Marcia and Rheasilvia terrains), and the Moon appear to have been hit by a projectile population with a similar shaped SFD for an extended period (see Sec. 3.4).

Dynamics of Near-Earth Objects

A comparison between the model predictions of Bottke et al. (2005b) and the observed NEO population discussed in the chapter by Harris et al. (Fig. 2) is intriguing for a different reason. The model does a reasonable job of fitting the observed data for small and larger NEOs, but there is a distinct mismatch near $D \sim 0.1$ km. The same kind of discrepancy is found between the model main belt and small craters on Vesta at the same approximate location when the craters are scaled back to projectiles (see chapter by Marchi et al.) (Fig. 5). This difference suggest the model is missing something:

1. YORP spin up torques produce such efficient mass shedding as asteroids sizes approach $D \sim 0.1$ km that they can influence the shape of the main belt SFD (Jacobson et al. 2014). This same mechanism, however, would need to shut off for $D < 0.1$ km. The reason why YORP mass shedding approaches termination is unknown, but we can think of several possibilities: (i) the physical nature and/or internal structure of small asteroids may be different than large asteroids, with smaller bodies less likely to be rubble-piles; (ii) small asteroids may be more susceptible to being held together by non-gravitational cohesive forces; or (iii) the thermal properties of the small asteroids are different than those of large asteroids and/or small asteroids become isothermal enough that the YORP mass shedding is less pronounced.

2. The Yarkovsky effect is more efficient at delivering small main belt asteroids to resonances than predicted by Bottke et al. (2005b). As more $D \sim 0.1$ km objects are evacuated from the main belt population, a steady-state deficit of small bodies may be created in of both the main belt and NEO populations near this size. The reason for this increased delivery efficiency may be related to the YORP shut down effects discussed above. If YORP becomes less efficient, bodies may become less likely to experience YORP cycles that can cause them to random walk in semimajor axis. In turn, this would enhance their escape rate out of the main belt.

These possibilities illustrate the importance of understanding all of the physical processes that affect small bodies in the inner solar system; they feedback in interesting ways, and they may ultimately affect how we interpret the ages of surfaces on both asteroids and the terrestrial planets. We look forward to seeing this investigated in the future.

Monolithic vs Rubble-pile Structure

Recent collisional modeling work by Cibulková et al. (2014) has also taken a more sophisticated look at the evolution of six different main belt regions (Fig. 11): inner, middle, "pristine", outer, Cybele zone, and a high-inclination region. Their goal was to fit the SFDs and asteroid families formed in all of these zones. The observed SFDs in these regions were computed from the available WISE satellite (Masiero et al., 2011; see chapter by Mainzer et al.). They also assumed the bodies were both monolithic asteroids and rubble piles, with the fragment SFDs derived from Durda et al. (2007) and Benavidez et al. (2012), respectively. Their work also allows for dynamical depletion due to the Yarkovsky effect.

Cibulková et al. (2014) found a number of intriguing results. First, Yarkovsky-driven depletion for small bodies is necessary to reproduce the observed main belt SFD in the size range tested: $D = 1$ to 10 km. Second, that treating all asteroids as weak rubble-piles as defined by Benavidez et al. (2012) led to SFDs that are too shallow below $D < 10$ km, as well as a factor of 2 more large families produced than are observed. This does not necessarily mean that asteroids are not rubble piles; an alternative would be that their disruption law is close to that derived for monolithic objects. New models of how porous rubble-pile asteroids break up suggest this may be the most likely answer (see chapter by Jutzi et al.). Third, Cibulková et al. also found that individual breakups are unlikely to change the SFDs of the regions they investigated. This is consistent with the main belt staying close to an equilibrium state, though certain perturbations can produce short-term changes to this state.

Finally, even at the current limit of observational completeness (3 to 6 km, depending on the main belt zone), the frequency of collisions becomes comparable to the dynamical removal of bodies by the Yarkovsky effect and major mean-motion resonances (Bottke et al. 2005a,b) or rotational disruption induced by the YORP effect (Jacobsen et al. 2014). Regarding the former effect, removal rates used by Bottke et al. (2005b) or those in Cibulková et al. (2014)

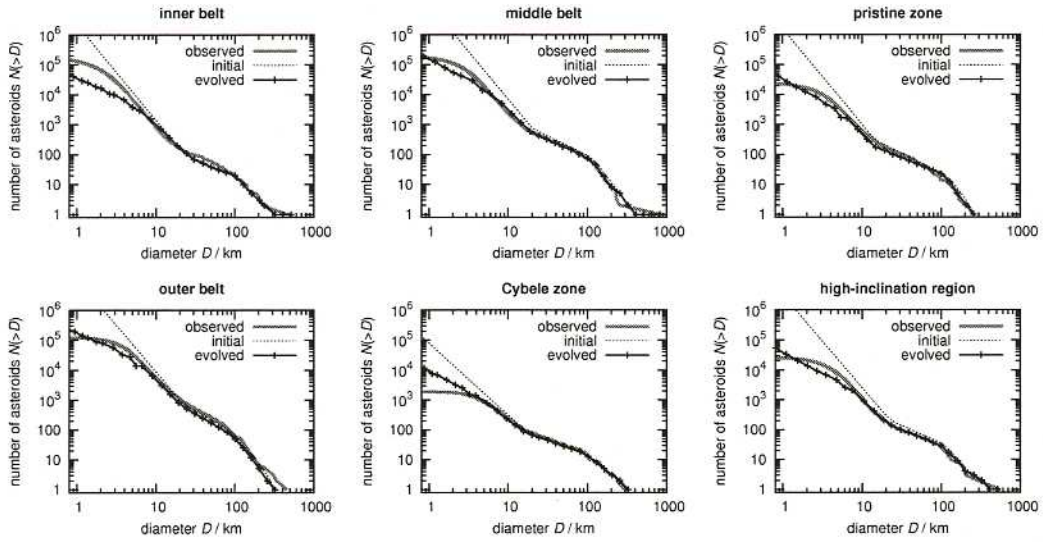

Fig. 11.— Observed size-frequency distributions (gray lines) for six parts of the main belt compared to simulated initial (dashed) and final SFDs (black), after 4 Gy of collisional evolution. This particular simulation shows the best-fit model out of more than 200,000 ones which were started with various initial conditions. We assumed the scaling law of Benz and Asphaug (1999) and a monolithic structure of bodies. The largest differences can be seen for the inner and outer belt; they can be attributed to a dynamical removal of small bodies ($D < 0.1$ km) caused by the Yarkovsky effect, which then cannot serve as projectiles for larger bodies ($\simeq 1$ km). Note that it is not easy to improve these results by increasing the normalization of the outer belt, because this would affect all of the remaining population as well. Adapted from Cibulková et al. (2014).

seem to be compatible with observations, namely the observed SFDs. The same may also be true for the latter process, though this will need to be examined in greater detail with the implications of Statler (2009) included. At this time, it is not clear which process dominates.

4.5 Connections between Asteroid Families and Meteorites

One of the most perplexing issues involving meteorite delivery concerns the fact that we currently have many tens of thousands of meteorites in worldwide collisions, yet this population could represent as few as $\sim$ 100 different asteroid parent bodies: $\sim$ 27 chondritic, $\sim$ 2 primitive achondritic, $\sim$ 6 differentiated achondritic, $\sim$ 4 stony-iron, $\sim$ 10 iron groups, and $\sim$ 50 ungrouped irons (e.g., Burbine et al. 2002). If we remove the stony-iron, iron, and differentiated meteorites, this number is reduced to as few as $\sim$ 30 parent bodies. This mismatch is even more puzzling given current meteorite delivery scenarios, where nearly any small main belt fragment can potentially reach a resonance capable of taking it into the terrestrial planet region via the Yarkovsky effect (see chapter by Vokrouhlický et al.). Presumably, this would suggest that our meteorite collisions should have samples from thousands upon thousands of distinct parent bodies.

An important missing component here is information on how collisional evolution has shaped meteorite delivery in the asteroid belt. Using the models discussed above, it is useful to apply what we have learned to the issue of stony meteoroid production, evolution, and delivery to the Earth. First, one can consider what happens when a body undergoes a cratering or catastrophic disruption event. A fragment SFD is created ranging from meteoroid-sized bodies all the way to multi-km asteroids (or more). Subsequent collisions onto bodies in the SFD act as a source for new meteoroids that are genetically the same as those created in the previous generation. This collisional cascade guarantees that some meteoroids from this family, representing a single parent body, will be provided to the main belt population, resonances, and possibly to Earth for an extended interval. At the same time, dynamical processes and collisions onto the newly-created meteoroids act as a sink to eliminate them from the main belt.

An example of this process is shown in Fig. 12. It shows what happens when fragment SFDs produced by $D = 30$ km and 100 km parent bodies are placed in the main belt $\sim$ 3.1 Gyr ago. For fragments derived from the 30 km body, the initial meteoroid population (i.e., the population of meter-sized bodies) drops by a factor of 100 and 10^5 within 130 Myr and within 3.1 Gy, respectively. Thus, meteoroid production by $D < 30$ km parent bodies decays away so quickly that ancient breakup events of this size are unlikely to deliver meaningful numbers of meteoroids to Earth today. For the 100 km parent body, the decay rate is significantly slower, with the meteoroid pop-

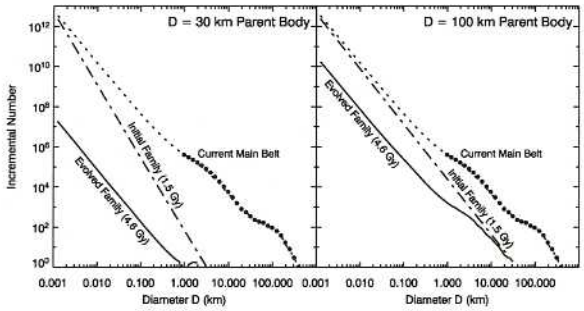

Fig. 12.— The collisional and dynamical evolution of two asteroid families with simple fragment SFDs produced by the disruption of a $D = 30$ and 100 km parent bodies (Bottke et al. 2005c). Both were inserted into the collision evolution model at 1.5 Gy after solar system formation. The meteoroid population is represented by the number of bodies in the $D \sim 0.001$ km size bin. The solid lines show the families at present (4.6 Gy). The smaller family has decayed significantly more than the larger family. Note the shallow slope of the $D = 100$ km family for $0.7 \lesssim D \lesssim 5$ km. This shape mimics the that of the background main belt population over the same size range.

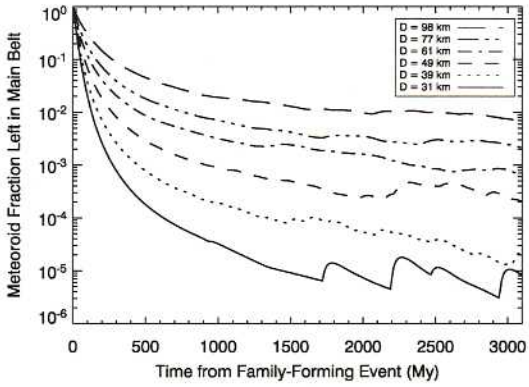

Fig. 13.— Decay rates of meteoroid populations from asteroid families with simple power law fragment SFD produced from parent bodies between $30 < D < 100$ km. All families were inserted in collisional model at 3.1 Gyr ago. The meteoroid population in the smallest families decrease by a factor of 100 over a few 0.1 Gyr while the largest take several Gyr to decay by the same factor.

ulation only dropping by a factor of 100 over 2-3 Gy. This suggests that many meteoroids reaching Earth today could come from prominent asteroid families with sizable SFDs, even if those families were created billions of years ago.

Bottke et al. (2005c) used these ideas to estimate how many stony meteorite classes should be in our collection. They did this by computing the meteoroid decay rates taken from different parent body sizes (Fig. 13) and combining it with the estimated production rate of asteroid families over the last ~ 4 Gyr. This calculation made many simplifying assumptions: (i) meteoroids from all parts of the main belt have an equal chance of reaching Earth, (ii) all $D > 30$ km asteroids disrupted over the last several Gyr have the capability of producing a distinct class of meteorites, and (iii) once a family's meteoroid production rate drops by a factor of 100, an arbitrary choice, it was unlikely to produce enough terrestrial meteorites to be noticed in our collection.

They found that asteroid families produced by the breakup of $D > 100$ km bodies have such slow meteoroid decay rates that most should be providing some meteoroids today, regardless of their disruption time over the last 3 Gyr. Among the smaller parent bodies ($30 < D < 100$ km), they found that, on average, the interval between disruption events across the main belt was short enough that many have disrupted over the last Gyr or so, enough to provide some meteoroids as well.

Overall, the found that stony meteorites were plausibly coming from ~ 45 different parent bodies. This value is fairly close to the actual value of ~ 30 parent bodies. A few reasons that the model estimate may be on the high side include: (i) some disruption events must occur within existing families, so no unique meteorite class would be created, and (ii) some outer main belt meteoroids may have great difficulty reaching Earth because they only have access to resonances that are orders of magnitude less efficient at delivering meteoroids to Earth than inner main belt resonances (Gladman et al. 1997; Bottke et al. 2006), and (iii) we have not factored in the different fragment SFD actual families can have. We conclude that most stony meteorites are byproducts of a collisional cascade, with some coming from asteroid families produced by the breakup of $D > 100$ km bodies over the last several Gyr and the remainder coming from smaller, more recent breakup events among $D < 100$ km asteroids that occurred over recent times (i.e., $\ll 1$ Gy).

4.5 Cometary impacts on main belt asteroids during the Late Heavy Bombardment

An interesting quandary comes from the predicted bombardment of comets on main belt asteroids during the Nice model (see chapter by Morbidelli et al.). According to Brož et al. (2013), a massive $25\,M_\oplus$ disk of trans-Neptunian comets might contain 10^{12} $D > 1$km comets. Using numerical simulations of Vokrouhlicky et al. (2008) and Minton and Malhotra (2010), they estimated the collision probabilities and impact velocities for comet hitting main belt asteroids to be $P_i \sim 6 \times 10^{-18}$ km^{-2} yr^{-1} and $V_{\rm imp} \sim 10$ km s^{-1}. Coupled with models describing the loss of asteroids during resonance sweeping, they estimated that the LHB could potentially disrupt as many as 100 parent bodies with $D_{\rm PB} > 100$ km, depending on the assumptions made (Fig. 14).

These values would violate many of the constraints provided in Sec. 3, and they present an intriguing challenge to the main tenets of the Nice model. One option here would be to reject the Nice model altogether, though this would also mean also giving up the features that made it com-

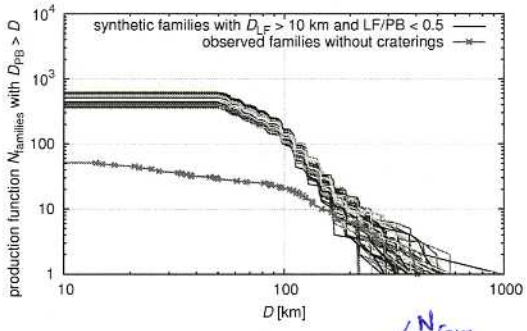

Fig. 14.— The outcomes of the bombardment of the main asteroid belt by trans-Neptunian comets, as modeled by Brož et al. (2013). The plot shows the family production functions (i.e. the cumulative number $N(>D)$ of families with parent-body size $D_{\rm PB}$ larger than D) and a comparison to the observed one. In order to distinguish 100 individual simulations (differing only by random-seed values) we plot them using lines of different colors, ranging from black to yellow.

pelling over the last decade (see chapter by Morbidelli et al.).

The other possibility is that there are aspects of the Nice model or our collision models that need revision. For example, the disk of trans-Neptunian comets may have different initial conditions than have been previously assumed, such that the collision probabilities between comets and asteroids are lower than expected (D. Nesvorný, personal communication). It is also possible that numerous trans-Neptunian comets disrupt when they enter the inner solar system due to volatile pressure build-up, amorphous/crystalline phase transitions, spin-up by jets, etc [REF]. Brož et al. (2013) examined this possibility by arbitrarily assuming that all comets disrupt at perihelion distance $q_{\rm crit} < 1.5$ AU. On average, this led to the correct number of catastrophic disruptions for $D_{\rm PB} = 200$ to 400 km bodies, but it still produced a factor of 2-3 more disruptions for $D_{\rm PB} \simeq 100$ km bodies than observed. These values assume, of course, that collisions between low density porous comets and asteroids are understood, when in reality no hydrocode simulations have ever runs using thi sset up. Finally, it could be that the main belt can accommodate more early collisions than predicted here. The constraints we have on the early era are extremely limited. All of these topics remain exciting areas for future research.

5. CONCLUSIONS

Considerable progress has been made over the last several decades in interpreting how the main belt reached its current state. We expect the next major advances will probably come from the inclusion of new and better constraints that can help modelers rule out possible solutions. A few of the entries on our wish list for new data includes: (i) increased information on the main belt population for $D < 1$ km bodies (e.g., albedos, colors, spectroscopy, sizes, etc.), (ii) a substantiated chronology for lunar and terrestrial crater populations, with crater SFD information verified for a wide range of surface ages, (iii) a thorough examination of the main belt for ghost families, (iv) more information on small asteroids that enable better predictions of Yarkovsky drift rates and YORP torques for $D < 1$ km asteroids, (v) additional non-saturated crater SFDs from asteroid surfaces, (vi) more discoveries of very young families, enough that we convince ourselves we have a complete set for a given time period.

In regards to modeling work, the next step major steps forward will probably come from next-generation codes that can track how asteroid populations move across the main belt via Yarkovsky/YORP forces while also undergoing comminution. This would allow the collisional cascade in the main belt to be treated as accurately as possible from disruption all the way to the fragments reaching resonances. Additional information on asteroids collisions at all sizes from numerical hydrocode simulations would be extremely useful, as would laboratory and numerical experiments completed on a wide range of asteroid compositions and internal structures. This would allow new codes to accurately account for the varying $Q^*_{\rm D}$ functions and fragment SFDs that asteroid families of different composition might have.

Finally, it is imperative that collisional models employ the best estimates of how the main belt and external small body populations have dynamically evolved with time. The history of our Solar System system is etched into the main belt population in enumerable ways, and the only way to read these markings and tell the story of our home is to unite models of collisional and dynamical evolution from the formation of the first solids all the way to the present day.

Acknowledgments. Research funds for William Bottke and Simone Marchi were provided by NASA's Solar System Evolution Research Virtual Institute (SSERVI) as part of the Institute for the Science of Exploration Targets (ISET) at the Southwest Research Institute (NASA grant number NNA14AB03A). The work of Miroslav Brož was supported by the Czech Grant Agency (grant no. P209-12-01308S).

Masiero, J., et al., 2011, Main belt asteroids with WISE/NEOWISE I: Preliminary albedos and diameters, *Astrophys. J.* **741**, 68 (20pp).

Marchi, S., and 11 colleagues 2012. The Violent Collisional History of Asteroid 4 Vesta. Science 336, 690-693.

Marchi, S., and 10 colleagues 2013. High-velocity collisions from the lunar cataclysm recorded in asteroidal meteorites. Nature Geoscience 6, 303-307.

Marzari, F., Rossi, A., Scheeres, D. J. 2011. Combined effect of YORP and collisions on the rotation rate of small Main Belt asteroids. Icarus 214, 622-631.

McEwen, A. S., Moore, J. M., Shoemaker, E. M. 1997. The Phanerozoic impact cratering rate: Evidence from the farside of the Moon. Journal of Geophysical Research 102, 9231-9242.

Melosh, H. J. 1989. Impact cratering: A geologic process. Oxford University Press (Oxford Monographs on Geology and Geophysics, No. 11), 1989, 253.

??erline, W. J., Weidenschilling, S. J., Durda, D. D., Margot, J. L., Pravec, P., Storrs, A. D. 2002. Asteroids Do Have Satellites. In *Asteroids III* (Eds. W.F. Bottke, A. Cellino, P. Paolicchi, and R.P. Binzel), University of Arizona Press, 289-312.

Minton, D. A., Malhotra, R. 2009. A record of planet migration in the main asteroid belt. Nature 457, 1109-1111.

Minton, D. A., Malhotra, R. 2011. Secular Resonance Sweeping of the Main Asteroid Belt During Planet Migration. The Astrophysical Journal 732, 53.

Morbidelli, A. and B. Gladman 1998. Orbital and temporal distributions of meteorites originating in the asteroid belt. Meteoritics and Planetary Science 33, 999-1016

Morbidelli, A. and D. Vokrouhlický 2003. The Yarkovsky-driven origin of near-Earth asteroids. Icarus 163, 120-134.

Morbidelli, A., Bottke, W. F., Nesvorný, D., Levison, H. F. 2009. Asteroids were born big. Icarus 204, 558-573.

Morbidelli, A., Brasser, R., Gomes, R., Levison, H. F., Tsiganis, K. 2010. Evidence from the Asteroid Belt for a Violent Past Evolution of Jupiter's Orbit. The Astronomical Journal 140, 1391-1401.

Morbidelli, A., Marchi, S., Bottke, W. F., Kring, D. A. 2012. A sawtooth-like timeline for the first billion years of lunar bombardment. Earth and Planetary Science Letters 355, 144-151.

Mothé-Diniz, T., Carvano, J. M. á., Lazzaro, D. 2003. Distribution of taxonomic classes in the main belt of asteroids. Icarus 162, 10-21.

Nesvorný, D., A. Morbidelli, D. Vokrouhlický, W. F. Bottke, and M. Brož 2002a. The Flora Family: A Case of the Dynamically Dispersed Collisional Swarm? Icarus 157, 155-172.

Nesvorný, D., Ferraz-Mello, S., Holman, M., Morbidelli, A. 2002b. Regular and Chaotic Dynamics in the Mean-Motion Resonances: Implications for the Structure and Evolution of the Asteroid Belt. In *Asteroids III* (Eds. W.F. Bottke, A. Cellino, P. Paolicchi, and R.P. Binzel), University of Arizona Press, 379-394.

Nesvorný, D., W. F. Bottke, H. Levison, and L. Dones. 2003. Recent origin of the solar system dust bands. Astrophys. J. 591, 486-497.

Nesvorný, D. and Bottke, W.F., 2004, Detection of the Yarkovsky effect for main-nelt asteroids, *Icarus* **170**, 324–342.

Nesvorný, D., Roig, F., Gladman, B., Lazzaro, D., Carruba, V., Mothé-Diniz, T. 2008. Fugitives from the Vesta family. Icarus 193, 85-95.

Nesvorný, D. 2011. Young Solar System's Fifth Giant Planet?. The Astrophysical Journal 742, L22.

Nesvorný, D., Morbidelli, A. 2012. Statistical Study of the Early Solar System's Instability with Four, Five, and Six Giant Planets. The Astronomical Journal 144, 117.

Novaković, B., Dell'Oro, A., Cellino, A., Knežević, Z. 2012. Recent collisional jet from a primitive asteroid. Monthly Notices of the Royal Astronomical Society 425, 338-346.

Novaković, B., Hsieh, H. H., Cellino, A., Micheli, M., Pedani, M. 2014. Discovery of a young asteroid cluster associated with P/2012 F5 (Gibbs). Icarus 231, 300-309.

O'Brien, D. P. and R. Greenberg 2003. Steady-state size distributions for collisional populations:analytical solution with size-dependent strength. Icarus 164, 334-345.

O'Brien, D. P., Morbidelli, A., and Levison, H. F. (2006). Terrestrial planet formation with strong dynamical friction. Icarus, 184, 39-58.

O'Brien, D. P., Morbidelli, A., and Bottke, W. F. (2007). The primordial excitation and clearing of the asteroid belt - Revisited. Icarus, 191, 43-452.

Opik, E. J. 1951. Collision probability with the planets and the distribution of planetary matter. Proc. R. Irish Acad. 54, 165-199.

Parker, A., Ivezić, Ž., Jurić, M., Lupton, R., Sekora, M.D. and Kowalski, A., 2008, The size distributions of asteroid families in the SDSS Moving Object Catalog 4, *Icarus* **198**, 138–155.

Petit, J., Chambers, J., Franklin, F., and Nagasawa, M. (2002). Primordial Excitation and Depletion of the Main Belt. In W. F. Bottke, A. Cellino, P. Paolicchi, and R. P. Binzel, editors, Asteroids III , pages 711-738. University of Arizona Press, Tucson, AZ.

Pravec, P., A. W. Harris, and T. Michalowski 2002. Asteroid Rotations. In Asteroids III, W. F. Bottke, A. Cellino, P. Paolicchi, R. Binzel, Eds. U. Arizona Press, 113-122.

Rabinowitz, D. L. E. Helin, K. Lawrence, and S. Pravdo. 2000. A Reduced Estimate of the Number of Kilometre-Sized Near-Earth Asteroids. Nature 403, 165-166

Robbins, S. J. 2014. New crater calibrations for the lunar crater-age chronology. Earth and Planetary Science Letters 403, 188-198.

Ryder, G., Bogard, D., Garrison, D. 1991. Probable age of Autolycus and calibration of lunar stratigraphy. Geology 19, 143-146.

Schenk, P., and 13 colleagues 2012. The Geologically Recent Giant Impact Basins at Vesta's South Pole. Science 336, 694-697.

Slivan, S. M. 2002. Spin vector alignment of Koronis family asteroids. Nature 419, 49-51.

Slivan, S. M., Molnar, L. A. 2012. Spin vectors in the Koronis family: III. (832) Karin. Icarus 220, 1097-1103.

Statler, T.S., 2009, Extreme sensitivity of the YORP effect to small-scale topography, *Icarus* **202**, 502–513.

Slivan, S. M., Binzel, R. P., Crespo da Silva, L. D., Kaasalainen, M., Lyndaker, M. M., Krčo, M. 2003. Spin vectors in the Koronis family: comprehensive results from two independent analyses of 213 rotation lightcurves. Icarus 162, 285-30

Stöffler, D., Ryder, G. 2001. Stratigraphy and Isotope Ages of Lunar Geologic Units: Chronological Standard for the Inner Solar System. Space Science Reviews 96, 9-54.

Stokes, G. H., D.K. Yeomans, W.F. Bottke, S.R. Chesley, J.B. Evans, R.E. Gold, A.W. Harris, D. Jewitt, T.S. Kelso, R.S. McMillan, T.B. Spahr, and S.P. Worden, *Report of the Near-Earth Object Science Definition Team: A Study to Determine the Feasibility of Extending the Search for Near-Earth Objects to Smaller Limiting Diameters.* NASA-OSS-Solar System Ex-